# Embedded Multiconductor Transmission Line Characterization

Dylan F. Williams, *Senior Member, IEEE*

***Abstract*- This paper presents a measurement method that characterizes lossy printed multiconductor transmission lines embedded in transitions, connectors, or packages with significant electrical parasitics. We test the method on a pair of lossy coupled asymmetric microstrip lines and compare to previous results.**

## INTRODUCTION

This paper extends the measurement method of Ref. [1] to the characterization of multiconductor transmission lines with parasitic elements between the measurement reference planes and the lines under test. It determines both the modal and "power-normalized" conductor quantities of [2] and [3] describing the line. We apply the method to a pair of lossy asymmetric coupled microstrip lines and compare it to the results of Ref. [1].

The characterization method of Ref. [1] determines quantities describing a multiconductor transmission line in its modal and conductor representations from two-port scattering-parameter measurements of multiple lengths of the line. However the method assumes that the electrical parasitics of the transitions between the measurement reference plane and the lines under test can be neglected. This limits the method to situations such as on-wafer characterization where these parasitics can be kept to a minimum; the method will fail for multiconductor lines embedded in packages or cables with connectors that have significant electrical parasitics.

Figure 1 illustrates the procedure of Ref. [1]. It begins with a multiline TRL calibration [4] with reference impedance correction [5] in the microstrip access lines. This calibration corrects for the imperfections in the analyzer and removes the effects of the wafer probes, via-hole transitions (not shown), and access lines used to connect the analyzer to the multiconductor lines: it also eliminates the need for the models required in Ref. [6] to account for the contacts and access lines.

The initial reference plane of the TRL calibration is in the middle of the shortest line, marked A in the upper box of Fig. 1. Measurements at the reference plane marked B in the upper box of Fig. 1 determine the impedances of the imperfect loads, which consisted of a section of the access line, a probe, and a coaxial load.

For each coupled line measurement the terminals at each of the analyzer measurement ports are connected between one of the conductors of the transmission line and its ground; the imperfect loads connect all of the remaining conductors at both the near and far ends of the line to

Reprinted from the 1997 IEEE MTT-S Digest, pp. 1773-1776, June 8-13, 1997. 

their grounds. This is illustrated in the lower box of Fig. 1, which shows one of the several ways in which the the analyzer and loads were connected to the lines. The weighted orthogonal distance regression algorithm of Ref. [7] finds the matrices of conductor transmission line impedances $\boldsymbol{Z}_c \equiv \boldsymbol{R}_c + j\omega\boldsymbol{L}_c$ and conductor admittances $\boldsymbol{Y}_c \equiv \boldsymbol{G}_c + j\omega\boldsymbol{C}_c$ per unit length that best reproduce the two-port measurements at reference plane C of Fig. 1 of the impedances of sections of the multiconductor transmission lines terminated with the imperfect loads.

The procedure of Ref. [1] cannot account for transition parasitics at or near measurement reference plane C. These transition parasitics include coupling between the access lines and parasitics at the bend where the access lines connect to the multiconductor transmission lines. This is because Ref. [1] fitted the multiconductor transmission line model in the upper part of Fig. 2, which does not include any transition parasitics, to the measurements.

Ref. [1] did not use a model with transition parasitics because the parameters needed for an electrical model that includes transition parasitics and arbitrary $\boldsymbol{Z}_c$ and $\boldsymbol{Y}_c$ cannot be determined from measurements of the line alone: there are a multiplicity of solutions for the electrical parameters describing the transition parasitics and transmission line parameters that have identical electrical behavior at the measurement reference planes C. Ref. [1] circumvented this limitation by reducing the transition parasitics to a minimum. However it is not always possible to reduce transition parasitics in connectorized cables and in multiconductor lines embedded in packages.

Here we use a new electrical model that properly accounts for transition parasitics. The new model is shown in the lower part of Fig. 2. Unlike the model of Ref. [1] (upper part of Fig. 2), it includes a general reciprocal four-port "error box" to account for the transition parasitics.

We also develop a new two-step procedure that avoids the problem of multiple solutions for the parameters $\boldsymbol{Z}_c$ and $\boldsymbol{Y}_c$ in the new and more complicated electrical model. The first step of the procedure is based on low-frequency approximations. While it does not determine $\boldsymbol{Z}_c$, $\boldsymbol{Y}_c$, or the parameters describing the transition parasitics accurately at high frequencies, we show that it works well enough at low frequencies to accurately determine $\boldsymbol{C}_{c0}$, the low-frequency limit of $\boldsymbol{C}_c$.

The second step of the procedure is based on the fact that $\boldsymbol{Y}_c$ is well approximated by $j\omega\boldsymbol{C}_{c0}$ over the entire band of measurement frequencies. Fixing $\boldsymbol{Y}_c$ in this second step allows all of the parameters of the electrical model that includes transition parasitics to be determined uniquely and accurately from the two-port measurements of the multiconductor transmission lines over a broad band of frequencies.

## MEASUREMENT PROCEDURE

The first step of the new two-step procedure is based on estimates of the impedance parameters of simple resistive circuits from dc measurements. The multiplicity of solutions for the parameters of the electrical model of the line and transition parasitics are eliminated in this step by adding measurements of these simple resistive circuits embedded in the multiconductor lines, as illustrated in the center box of Fig. 1, to the data set used in the optimization. However we also assume that the impedance parameters of the resistive circuits are equal to their dc values. Thus we expect this first step of the procedure to fail to accurately model the transmission line and transition parasitics at high frequencies, where we cannot accurately approximate the impedance parameters of the resistive circuits by their dc values. However, we anticipate that the model

would be accurate enough at low frequencies to determine $\boldsymbol{C}_{c0}$ by extrapolation of the approximate values of $\boldsymbol{C}_c$ to dc.

We used simulated data to test the new procedure. The two-port TRL measurement data was the same as that used in Ref. [1], except that we multiplied each of the scattering parameter measurements by the square of $0.5(1+j)$ to simulate the addition of an attenuator with 6 dB of loss and 45° of phase shift to the transition parasitics. This new data set was so corrupted by the addition of the simulated attenuators to the transition parasitics that the method of Ref. [1] failed to determine $\boldsymbol{Z}_c$ or $\boldsymbol{Y}_c$ even approximately.

Fig. 3 shows that estimates of the elements of $\boldsymbol{C}_c$ from the first step of the new procedure applied to the simulated data set compares well with the measurements of $\boldsymbol{C}_c$ determined by the method of Ref. [1] from the original uncorrupted data and with calculations from the full-wave method of Ref. [8]; it is quite easy to determine $\boldsymbol{C}_{c0}$ by extrapolation of $\boldsymbol{C}_c$ to dc from the data. In fact, the agreement between extrapolated values of $\boldsymbol{C}_c$ and those determined from the original uncorrupted data and the method of Ref. [1] was better than 2%.

## MEASUREMENT OF $\boldsymbol{Z}_c$

The second step of the new procedure measures $\boldsymbol{Z}_c$. To determine $\boldsymbol{Z}_c$ from the simulated data with 6 dB, 45° attenuators added to the transition parasitics we assumed that $\boldsymbol{Y}_c$ was well approximated by $j\omega\boldsymbol{C}_{c0}$: we verified the assumption $\boldsymbol{Y}_c \approx j\omega\boldsymbol{C}_{c0}$ with field calculations using the full-wave method of [8]. This assumption, like the addition of the resistive circuits in the first step, eliminates the multiplicity of solutions in the more complicated model that includes the transitions.

However in this second step we use only the measurements of sections of the multiconductor transmission line, as illustrated in the lower box of Fig. 1: this avoids the low frequency approximations required in the first step of the procedure and yields accurate results over the entire band of measurement frequencies.

Figure 4 compares the elements of $\boldsymbol{L}_c$ determined by this new procedure from our simulated data with 6 dB, 45° attenuators added to the transition parasitics to those determined by the method of Ref. [1] from the original uncorrupted data. The figure again shows good agreement, even at high frequencies, and demonstrates the accuracy of the method. The agreement between the elements of $\boldsymbol{R}_c$ determined by the two methods was also good.

## MODAL QUANTITIES

The microstrip coupled lines investigated here support two dominant quasi-TEM modes, which are commonly called the *c* and π modes, and which correspond to the even and the odd mode of the symmetric case, respectively. We determined the modal parameters describing the multiconductor transmission line from $\boldsymbol{Z}_c$ and $\boldsymbol{Y}_c$ using the procedure of Refs. [1] and [2]. Figure 5 shows that the modal propagation constants determined by the two methods agree well.

Figure 6 shows the modal cross-powers measured by the new algorithm reported here; as predicted by Ref. [9] the measured modal cross-powers are large. The figure shows better agreement between the modal cross-powers measured by the new algorithm and calculation using the full-wave method of Ref. [8] than was reported in Ref. [1]. This shows that the new

procedure applied to the simulated data with 6 dB, 45° attenuators added to the transition parasitics actually resulted in more accurate measurements than the procedure of Ref. [1] applied to the original uncorrupted data. This indicates that the new procedure corrects not only for the simulated attenuators but also for the small transition parasitics in the original uncorrupted data and suggests that the new procedure is more accurate than the old one even when transition parasitics are small.

## CONCLUSION

We presented a method for the measurement and characterization of lossy asymmetric printed multiconductor transmission lines that accounts for parasitics at the measurement reference planes. The method can also improve accuracy and should find application in the characterization of packaged multiconductor transmission lines and connectorized cables, which cannot be analyzed with the method of Ref. [1].

## ACKNOWLEDGMENTS

The author appreciates the contributions of Stefaan Sercu and Luc Martens at the University of Ghent in Ghent, Belgium, who made possible the measurements reported here.

## REFERENCES


[1] D. F. Williams, "Multiconductor Transmission Line Characterization," submitted to *IEEE Trans. Comp. Packag. Manufact. Technol.*

[2] D. F. Williams, L. A. Hayden, and R. B. Marks, "A complete multimode equivalent-circuit theory for electrical design," to be published in *J. Res. Natl. Inst. Stand. Technol.*

[3] N. Faché and D. De Zutter, "New high-frequency circuit model for coupled lossless and lossy waveguide structures," *IEEE Trans. Microwave Theory Tech.*, pp. 252-259, March 1990.

[4] R. B. Marks, "A Multiline Method of Network Analyzer Calibration," *IEEE Trans. Microwave Theory Tech.*, pp. 1205-1215, July 1991.

[5] R. B. Marks and D. F. Williams, "Characteristic Impedance Determination using Propagation Constant Measurement," *IEEE Microwave Guided Wave Lett.*, pp. 141-143, June 1991.

[6] T. Winkel, L.S. Dutta, H. Grabinski, E. Grotelueschen, "Determination of the Propagation Constant of Coupled Lines on Chips Based on High Frequency Measurements," *IEEE Multi-Chip Module Conf. Dig.*, Santa Cruz (CA), pp.99-104, 6-7 February, 1996.

[7] P.T. Boggs, R. H. Byrd, and R. D. Schnabel, "A stable and efficient algorithm for nonlinear orthogonal distance regression," *SIAM J. Sci. and Stat. Comp.*, pp. 1052-1078, Nov. 1987.

[8] W. Heinrich, "Full-wave analysis of conductor losses on MMIC transmission lines," *IEEE Trans. Microwave Theory Tech.*, pp. 1468-1472, Oct. 1990.

[9] D. F. Williams and F. Olyslager, "Modal cross power in quasi-TEM transmission lines," *IEEE Microwave Guided Wave Lett.*, pp. 413-415, Nov. 1996.

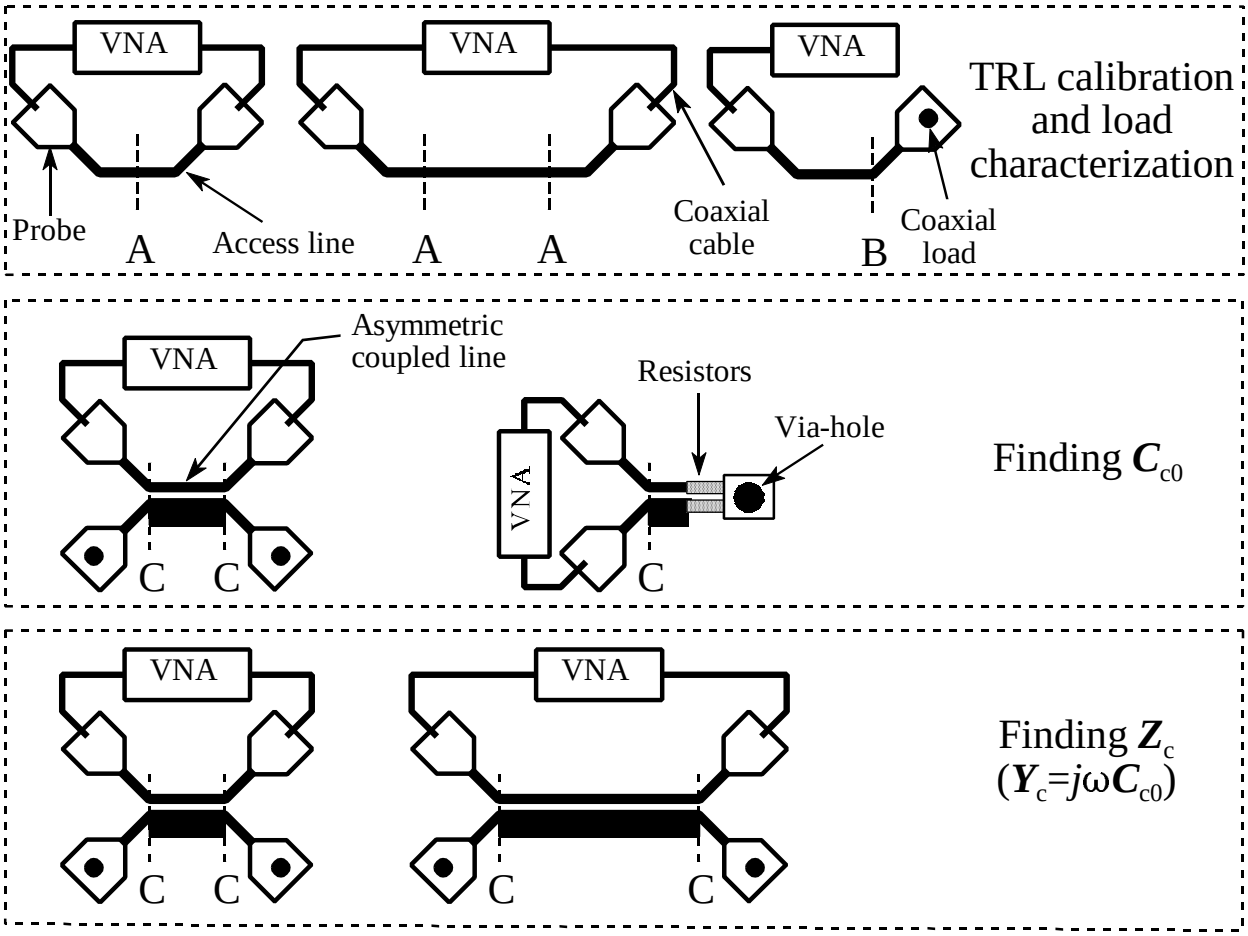


Fig. 1. A schematic representation of the measurement artifacts and procedure. Coaxial cables connect the vector network analyzer (VNA) to the ground-signal-ground probes. The probes contact the center conductor of the access lines directly; the ground contact is made with metallized via-holes, which are not shown in the figure.

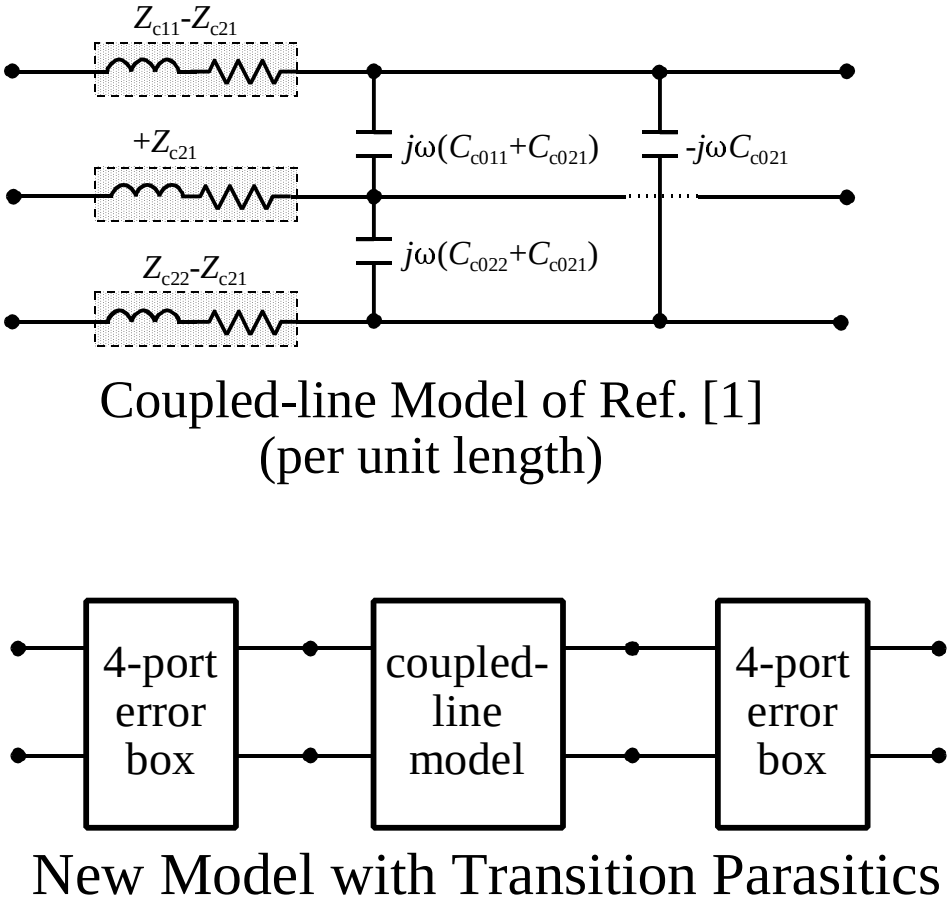


Fig. 2. The equivalent circuit model used in Ref. [1] is shown at the top of the figure; it does not account for transition parasitics. The new model used with the procedure described here is shown in the lower portion of the figure; it includes a reciprocal four-port error box to account for transition parasitics.

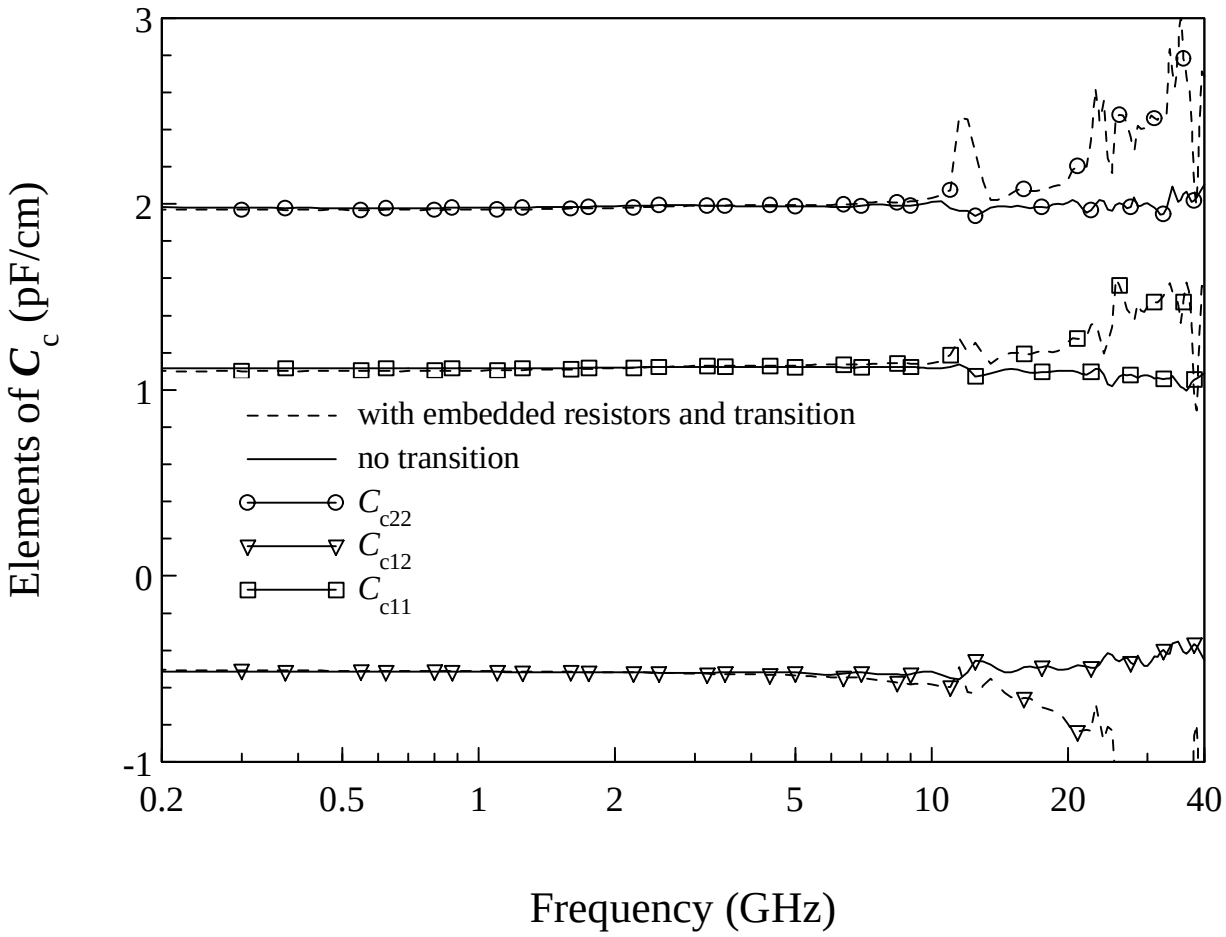


Fig. 3. Measurements of the elements of $\boldsymbol{C}_c$ determined from simulated data with 6 dB, 45° attenuators added to the transition parasitics are compared to results using the method of Ref. [1]. The coupled microstrip lines had widths of 54 µm and 254 µm separated by a gap of 45 µm printed on an alumina substrate with an approximate thickness of 254 µm. The conductor metalization had a measured thickness of 1.8 µm and dc conductivity of $3.3 \times 10^7$ $\Omega^{-1} \cdot m^{-1}$.

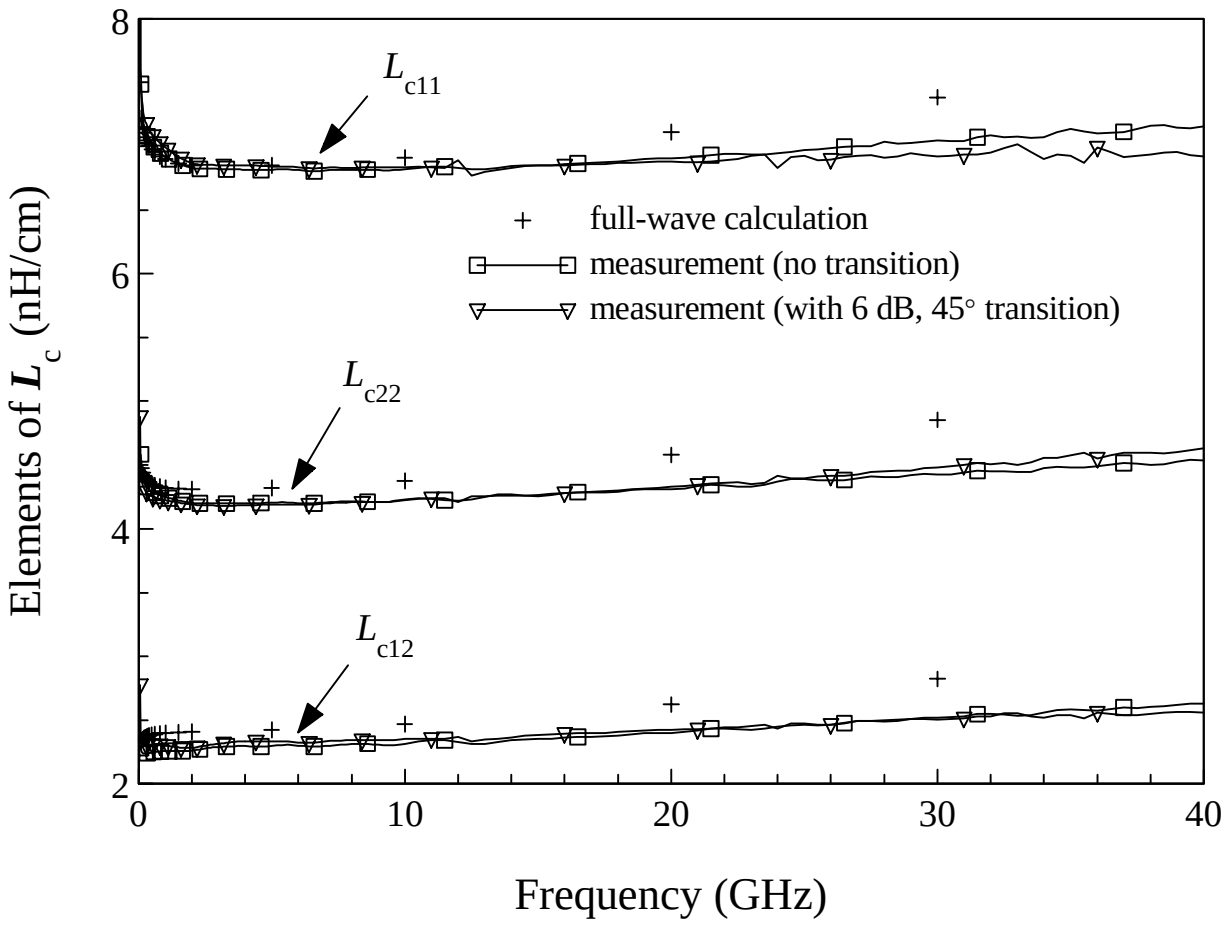


Fig. 4. Measurements of the elements of $\boldsymbol{L}_c$ are compared to full-wave calculations.

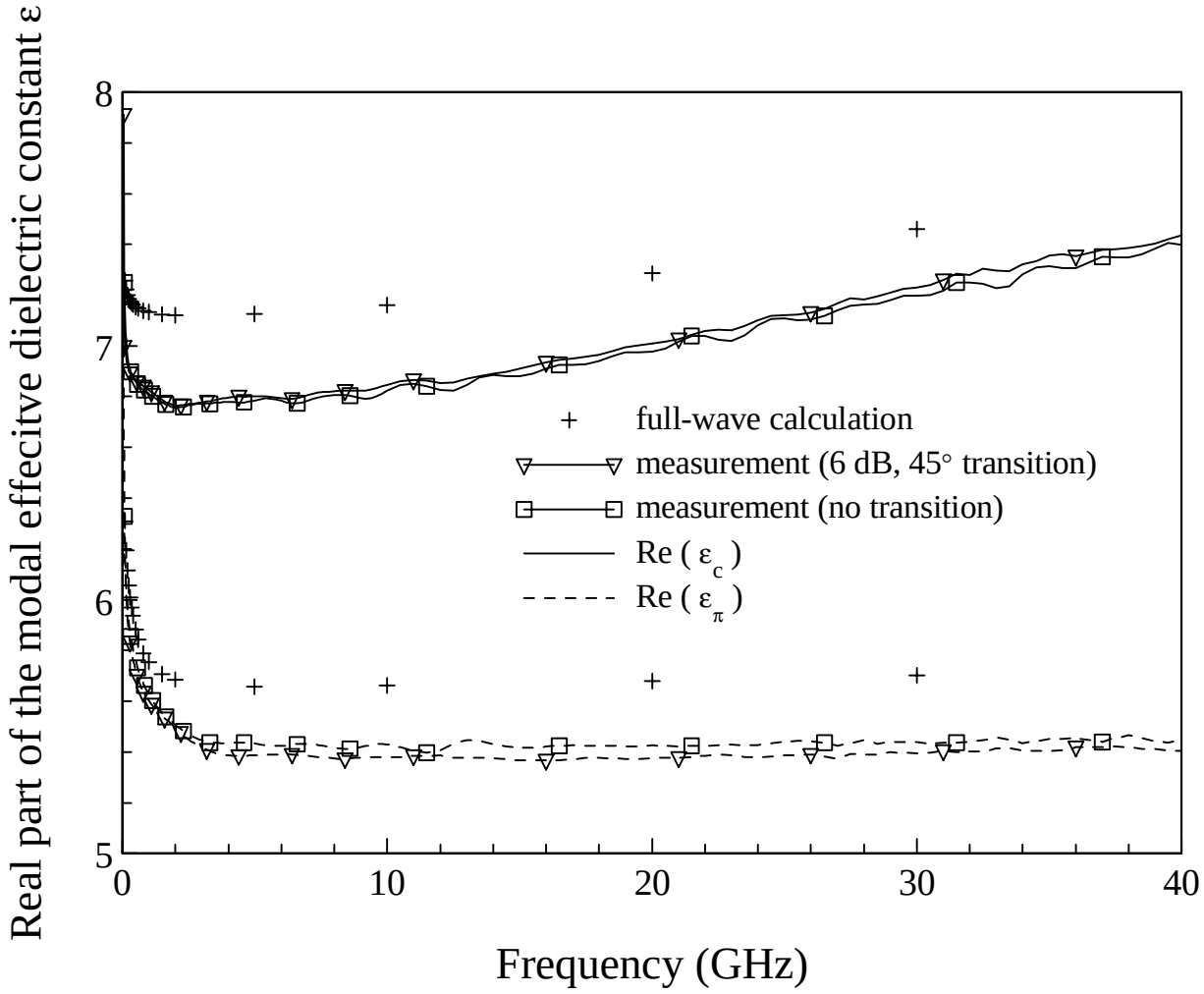


Fig. 5. Measurements of the real part of the modal effective dielectric constants are compared to full-wave calculations.

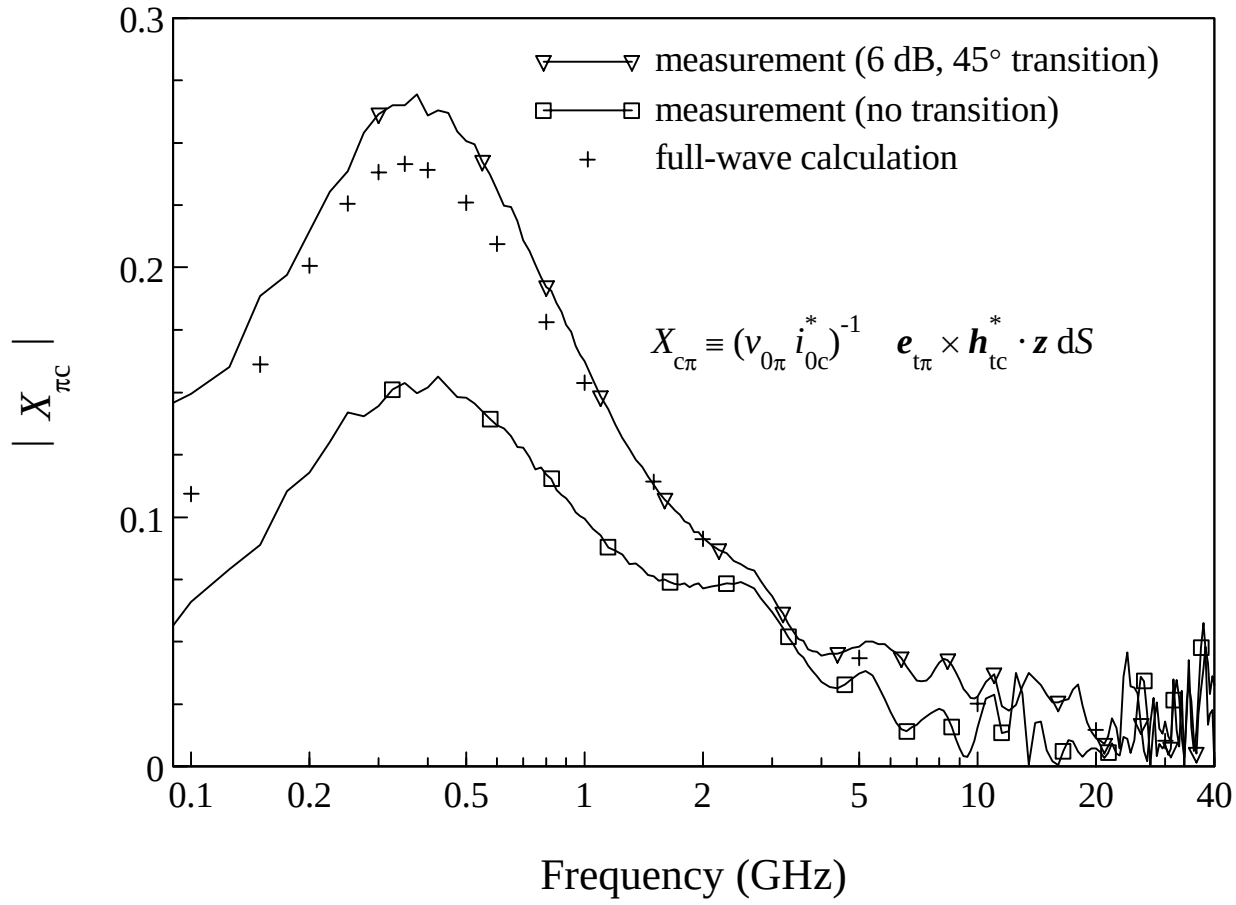


Fig. 6. Measurements of the magnitudes of the modal cross-powers are compared to full-wave calculations.